Elliptic Flow of Identified Hadrons in Au+Au Collisions at $\sqrt{s_{\rm NN}} = 200$ GeV

S.S. Adler,[5] S. Afanasiev,[17] C. Aidala,[5] N.N. Ajitanand,[43] Y. Akiba,[20,38] J. Alexander,[43] R. Amirikas,[12] L. Aphecetche,[45] S.H. Aronson,[5] R. Averbeck,[44] T.C. Awes,[35] R. Azmoun,[44] V. Babintsev,[15] A. Baldisseri,[10] K.N. Barish,[6] P.D. Barnes,[27] B. Bassalleck,[33] S. Bathe,[30] S. Batsouli,[9] V. Baublis,[37] A. Bazilevsky,[39,15] S. Belikov,[16,15] Y. Berdnikov,[40] S. Bhagavatula,[16] J.G. Boissevain,[27] H. Borel,[10] S. Borenstein,[25] M.L. Brooks,[27] D.S. Brown,[34] N. Bruner,[33] D. Bucher,[30] H. Buesching,[30] V. Bumazhnov,[15] G. Bunce,[5,39] J.M. Burward-Hoy,[26,44] S. Butsyk,[44] X. Camard,[45] J.-S. Chai,[18] P. Chand,[4] W.C. Chang,[2] S. Chernichenko,[15] C.Y. Chi,[9] J. Chiba,[20] M. Chiu,[9] I.J. Choi,[52] J. Choi,[19] R.K. Choudhury,[4] T. Chujo,[5] V. Cianciolo,[35] Y. Cobigo,[10] B.A. Cole,[9] P. Constantin,[16] D.G. d'Enterria,[45] G. David,[5] H. Delagrange,[45] A. Denisov,[15] A. Deshpande,[39] E.J. Desmond,[5] O. Dietzsch,[41] O. Drapier,[25] A. Drees,[44] R. du Rietz,[29] A. Durum,[15] D. Dutta,[4] Y.V. Efremenko,[35] K. El Chenawi,[49] A. Enokizono,[14] H. En'yo,[38,39] S. Esumi,[48] L. Ewell,[5] D.E. Fields,[33,39] F. Fleuret,[25] S.L. Fokin,[23] B.D. Fox,[39] Z. Fraenkel,[51] J.E. Frantz,[9] A. Franz,[5] A.D. Frawley,[12] S.-Y. Fung,[6] S. Garpman,[29,*] T.K. Ghosh,[49] A. Glenn,[46] G. Gogiberidze,[46] M. Gonin,[25] J. Gosset,[10] Y. Goto,[39] R. Granier de Cassagnac,[25] N. Grau,[16] S.V. Greene,[49] M. Grosse Perdekamp,[39] W. Guryn,[5] H.-Å. Gustafsson,[29] T. Hachiya,[14] J.S. Haggerty,[5] H. Hamagaki,[8] A.G. Hansen,[27] E.P. Hartouni,[26] M. Harvey,[5] R. Hayano,[8] X. He,[13] M. Heffner,[26] T.K. Hemmick,[44] J.M. Heuser,[44] M. Hibino,[50] J.C. Hill,[16] W. Holzmann,[43] K. Homma,[14] B. Hong,[22] A. Hoover,[34] T. Ichihara,[38,39] V.V. Ikonnikov,[23] K. Imai,[24,38] L.D. Isenhower,[1] M. Ishihara,[38] M. Issah,[43] A. Isupov,[17] B.V. Jacak,[44] W.Y. Jang,[22] Y. Jeong,[19] J. Jia,[44] O. Jinnouchi,[38] B.M. Johnson,[5] S.C. Johnson,[26] K.S. Joo,[31] D. Jouan,[36] S. Kametani,[8,50] N. Kamihara,[47,38] J.H. Kang,[52] S.S. Kapoor,[4] K. Katou,[50] S. Kelly,[9] B. Khachaturov,[51] A. Khanzadeev,[37] J. Kikuchi,[50] D.H. Kim,[31] D.J. Kim,[52] D.W. Kim,[19] E. Kim,[42] G.-B. Kim,[25] H.J. Kim,[52] E. Kistenev,[5] A. Kiyomichi,[48] K. Kiyoyama,[32] C. Klein-Boesing,[30] H. Kobayashi,[38,39] L. Kochenda,[37] V. Kochetkov,[15] D. Koehler,[33] T. Kohama,[14] M. Kopytine,[44] D. Kotchetkov,[6] A. Kozlov,[51] P.J. Kroon,[5] C.H. Kuberg,[1,27] K. Kurita,[39] Y. Kuroki,[48] M.J. Kweon,[22] Y. Kwon,[52] G.S. Kyle,[34] R. Lacey,[43] V. Ladygin,[17] J.G. Lajoie,[16] A. Lebedev,[16,23] S. Leckey,[44] D.M. Lee,[27] S. Lee,[19] M.J. Leitch,[27] X.H. Li,[6] H. Lim,[42] A. Litvinenko,[17] M.X. Liu,[27] Y. Liu,[36] C.F. Maguire,[49] Y.I. Makdisi,[5] A. Malakhov,[17] V.I. Manko,[23] Y. Mao,[7,38] G. Martinez,[45] M.D. Marx,[44] H. Masui,[48] F. Matathias,[44] T. Matsumoto,[8,50] P.L. McGaughey,[27] E. Melnikov,[15] F. Messer,[44] Y. Miake,[48] J. Milan,[43] T.E. Miller,[49] A. Milov,[44,51] S. Mioduszewski,[5] R.E. Mischke,[27] G.C. Mishra,[13] J.T. Mitchell,[5] A.K. Mohanty,[4] D.P. Morrison,[5] J.M. Moss,[27] F. Mühlbacher,[44] D. Mukhopadhyay,[51] M. Muniruzzaman,[6] J. Murata,[38,39] S. Nagamiya,[20] J.L. Nagle,[9] T. Nakamura,[14] B.K. Nandi,[6] M. Nara,[48] J. Newby,[46] P. Nilsson,[29] A.S. Nyanin,[23] J. Nystrand,[29] E. O'Brien,[5] C.A. Ogilvie,[16] H. Ohnishi,[5,38] I.D. Ojha,[49,3] K. Okada,[38] M. Ono,[48] V. Onuchin,[15] A. Oskarsson,[29] I. Otterlund,[29] K. Oyama,[8] K. Ozawa,[8] D. Pal,[51] A.P.T. Palounek,[27] V.S. Pantuev,[44] V. Papavassiliou,[34] J. Park,[42] A. Parmar,[33] S.F. Pate,[34] T. Peitzmann,[30] J.-C. Peng,[27] V. Peresedov,[17] C. Pinkenburg,[5] R.P. Pisani,[5] F. Plasil,[35] M.L. Purschke,[5] A. Purwar,[44] J. Rak,[16] I. Ravinovich,[51] K.F. Read,[35,46] M. Reuter,[44] K. Reygers,[30] V. Riabov,[37,40] Y. Riabov,[37] G. Roche,[28] A. Romana,[25] M. Rosati,[16] P. Rosnet,[28] S.S. Ryu,[52] M.E. Sadler,[1] N. Saito,[38,39] T. Sakaguchi,[8,50] M. Sakai,[32] S. Sakai,[48] V. Samsonov,[37] L. Sanfratello,[33] R. Santo,[30] H.D. Sato,[24,38] S. Sato,[5,48] S. Sawada,[20] Y. Schutz,[45] V. Semenov,[15] R. Seto,[6] M.R. Shaw,[1,27] T.K. Shea,[5] T.-A. Shibata,[47,38] K. Shigaki,[14,20] T. Shiina,[27] C.L. Silva,[41] D. Silvermyr,[27,29] K.S. Sim,[22] C.P. Singh,[3] V. Singh,[3] M. Sivertz,[5] A. Soldatov,[15] R.A. Soltz,[26] W.E. Sondheim,[27] S.P. Sorensen,[46] I.V. Sourikova,[5] F. Staley,[10] P.W. Stankus,[35] E. Stenlund,[29] M. Stepanov,[34] A. Ster,[21] S.P. Stoll,[5] T. Sugitate,[14] J.P. Sullivan,[27] E.M. Takagui,[41] A. Taketani,[38,39] M. Tamai,[50] K.H. Tanaka,[20] Y. Tanaka,[32] K. Tanida,[38] M.J. Tannenbaum,[5] P. Tarján,[11] J.D. Tepe,[1,27] T.L. Thomas,[33] J. Tojo,[24,38] H. Torii,[24,38] R.S. Towell,[1] I. Tserruya,[51] H. Tsuruoka,[48] S.K. Tuli,[3] H. Tydesjö,[29] N. Tyurin,[15] H.W. van Hecke,[27] J. Velkovska,[5,44] M. Velkovsky,[44] L. Villatte,[46] A.A. Vinogradov,[23] M.A. Volkov,[23] E. Vznuzdaev,[37] X.R. Wang,[13] Y. Watanabe,[38,39] S.N. White,[5] F.K. Wohn,[16] C.L. Woody,[5] W. Xie,[6] Y. Yang,[7] A. Yanovich,[15] S. Yokkaichi,[38,39] G.R. Young,[35] I.E. Yushmanov,[23] W.A. Zajc,[9,†] C. Zhang,[9] S. Zhou,[7,51] L. Zolin,[17]

(PHENIX Collaboration)

[1] *Abilene Christian University, Abilene, TX 79699, USA*
[2] *Institute of Physics, Academia Sinica, Taipei 11529, Taiwan*
[3] *Department of Physics, Banaras Hindu University, Varanasi 221005, India*
[4] *Bhabha Atomic Research Centre, Bombay 400 085, India*
[5] *Brookhaven National Laboratory, Upton, NY 11973-5000, USA*
[6] *University of California - Riverside, Riverside, CA 92521, USA*
[7] *China Institute of Atomic Energy (CIAE), Beijing, People's Republic of China*
[8] *Center for Nuclear Study, Graduate School of Science, University of Tokyo, 7-3-1 Hongo, Bunkyo, Tokyo 113-0033, Japan*
[9] *Columbia University, New York, NY 10027 and Nevis Laboratories, Irvington, NY 10533, USA*
[10] *Dapnia, CEA Saclay, Bat. 703, F-91191, Gif-sur-Yvette, France*

[11] Debrecen University, H-4010 Debrecen, Egyetem tér 1, Hungary
[12] Florida State University, Tallahassee, FL 32306, USA
[13] Georgia State University, Atlanta, GA 30303, USA
[14] Hiroshima University, Kagamiyama, Higashi-Hiroshima 739-8526, Japan
[15] Institute for High Energy Physics (IHEP), Protvino, Russia
[16] Iowa State University, Ames, IA 50011, USA
[17] Joint Institute for Nuclear Research, 141980 Dubna, Moscow Region, Russia
[18] KAERI, Cyclotron Application Laboratory, Seoul, South Korea
[19] Kangnung National University, Kangnung 210-702, South Korea
[20] KEK, High Energy Accelerator Research Organization, Tsukuba-shi, Ibaraki-ken 305-0801, Japan
[21] KFKI Research Institute for Particle and Nuclear Physics (RMKI), H-1525 Budapest 114, POBox 49, Hungary
[22] Korea University, Seoul, 136-701, Korea
[23] Russian Research Center "Kurchatov Institute", Moscow, Russia
[24] Kyoto University, Kyoto 606, Japan
[25] Laboratoire Leprince-Ringuet, Ecole Polytechnique, CNRS-IN2P3, Route de Saclay, F-91128, Palaiseau, France
[26] Lawrence Livermore National Laboratory, Livermore, CA 94550, USA
[27] Los Alamos National Laboratory, Los Alamos, NM 87545, USA
[28] LPC, Université Blaise Pascal, CNRS-IN2P3, Clermont-Fd, 63177 Aubiere Cedex, France
[29] Department of Physics, Lund University, Box 118, SE-221 00 Lund, Sweden
[30] Institut fuer Kernphysik, University of Muenster, D-48149 Muenster, Germany
[31] Myongji University, Yongin, Kyonggido 449-728, Korea
[32] Nagasaki Institute of Applied Science, Nagasaki-shi, Nagasaki 851-0193, Japan
[33] University of New Mexico, Albuquerque, NM, USA
[34] New Mexico State University, Las Cruces, NM 88003, USA
[35] Oak Ridge National Laboratory, Oak Ridge, TN 37831, USA
[36] IPN-Orsay, Universite Paris Sud, CNRS-IN2P3, BP1, F-91406, Orsay, France
[37] PNPI, Petersburg Nuclear Physics Institute, Gatchina, Russia
[38] RIKEN (The Institute of Physical and Chemical Research), Wako, Saitama 351-0198, JAPAN
[39] RIKEN BNL Research Center, Brookhaven National Laboratory, Upton, NY 11973-5000, USA
[40] St. Petersburg State Technical University, St. Petersburg, Russia
[41] Universidade de São Paulo, Instituto de Física, Caixa Postal 66318, São Paulo CEP05315-970, Brazil
[42] System Electronics Laboratory, Seoul National University, Seoul, South Korea
[43] Chemistry Department, Stony Brook University, SUNY, Stony Brook, NY 11794-3400, USA
[44] Department of Physics and Astronomy, Stony Brook University, SUNY, Stony Brook, NY 11794, USA
[45] SUBATECH (Ecole des Mines de Nantes, CNRS-IN2P3, Université de Nantes) BP 20722 - 44307, Nantes, France
[46] University of Tennessee, Knoxville, TN 37996, USA
[47] Department of Physics, Tokyo Institute of Technology, Tokyo, 152-8551, Japan
[48] Institute of Physics, University of Tsukuba, Tsukuba, Ibaraki 305, Japan
[49] Vanderbilt University, Nashville, TN 37235, USA
[50] Waseda University, Advanced Research Institute for Science and Engineering, 17 Kikui-cho, Shinjuku-ku, Tokyo 162-0044, Japan
[51] Weizmann Institute, Rehovot 76100, Israel
[52] Yonsei University, IPAP, Seoul 120-749, Korea
(February 8, 2008)

The anisotropy parameter (v_2), the second harmonic of the azimuthal particles distribution, has been measured with the PHENIX detector in Au+Au collisions at $\sqrt{s_{NN}} = 200$ GeV for identified and inclusive charged particle production at central rapidities ($|\eta| < 0.35$) with respect to the reaction plane defined at high rapidities ($|\eta| = 3$–4). We observe that the v_2 of mesons falls below that of (anti)baryons for $p_{\rm T} > 2$ GeV/c, in marked contrast to the predictions of a hydrodynamical model. A quark coalescence model is also investigated.

PACS numbers: 25.75.Dw

Event anisotropy is expected to be sensitive to the early stage of ultra-relativistic nuclear collisions at the Relativistic Heavy Ion Collider (RHIC). The possible formation of a quark-gluon plasma (QGP) could affect how the initial anisotropy in coordinate space is transferred into momentum space in the final state. The anisotropy parameter v_2 for a selection of produced particles is derived from the azimuthal distribution of those particles.

$$\frac{dN}{d\phi} \propto 1 + 2\,v_2 \cos 2(\phi - \Phi_{\rm RP}) \qquad (1)$$

where ϕ is the azimuthal direction of the particle and $\Phi_{\rm RP}$ is the direction of the nuclear impact parameter ("reaction plane") in a given collision. Measurements of the parameter v_2 in RHIC collisions have been performed [1–6] for charged particles and for identified particles. The current work reports results for charged particles versus transverse momentum ($p_{\rm T}$) out to 5 GeV/c, and extends previous measurements for identified particles out to 3 GeV/c for π and K, and to 4 GeV/c for protons. (Previous measurements of the v_2 for π, K, and p extended to 1 GeV/c at $\sqrt{s_{_{NN}}} = 130$ GeV. [2]) Detailed measurements of the azimuthal anisotropy are important to eventually discriminate among different possible scenarios for its physical origin. Such scenarios include: hydrodynamical flow of compressed hadronic matter, the production of multiple mini-jets, and an anisotropy developed during an early quark-matter phase of the collision. It has been observed that v_2 saturates at $p_{\rm T} \sim 2$ GeV/c and above [4,5]. The cause of this saturation is not yet known; however, we note that at this momentum the particle composition is very different than at low momentum in that the proton yield is comparable to the pion yield [7]. This makes the measurement of v_2 for separately identified particles especially interesting.

The measurements described here were carried out in the PHENIX experiment at RHIC [8]. About 28 M minimum bias Au+Au collisions at $\sqrt{s_{\rm NN}} = 200$ GeV from the 2001-2002 run period (Run-2) are used in the analysis. Charged particles are measured in the central arm spectrometers ($|\eta| < 0.35$) [9] where PHENIX has excellent particle identification capabilities [10]. The drift chamber (DC) and the first pad chamber plane (PC1) together with the collision vertex define the charged particle tracks. In order to reduce background, the reconstructed tracks are confirmed by requiring matching hits in the outer detectors, *i.e.* the third pad chamber plane (PC3) and the electromagnetic calorimeter (EMCAL) or the time-of-flight detector (TOF). In this analysis, the TOF detector is used to identify charged particles up to 4 GeV/c in $p_{\rm T}$. Particle time-of-flight is measured using the TOF with respect to the collision time defined by beam counters (BBC), and is used to calculate mass squared using the particle momentum and the flight path length [7]. The timing resolution of the system is $\simeq 120$ ps. A momentum dependent $\pm 2\ \sigma$ cut on mass squared allows particle identification in the $p_{\rm T}$ range $0.2 < p_{\rm T} < 3$ GeV/c for pions, $0.3 < p_{\rm T} < 3$ GeV/c for kaons, and $0.5 < p_{\rm T} < 4$ GeV/c for protons. The contamination of mis-identified particles is less than 10%. In addition to collision time, the BBC provide z-vertex position information. The two beam counters are located at $|z|$=1.5 m from the collision point, covering $|\eta| = 3 \sim 4$. They consist of 64 photo-multiplier tubes (PMT) equipped with quartz Cherenkov radiators in front surrounding the beam pipe. The large charged multiplicity (a few hundred) in $|\eta| = 3 \sim 4$ and the non-zero signal of event anisotropy in this η range enables us to estimate the azimuthal angle of the reaction plane in each event using the BBC with full azimuthal angle coverage.

Since the v_2 parameter is in effect a quadrupole moment, the anisotropy which gives rise to a non-zero v_2 is often referred to as an "elliptic flow." It is extracted by first determining the reaction plane angle $\Phi_{\rm RP}$ for each event,

$$\tan 2\Phi_{\rm RP} = \frac{\Sigma n_{\rm ch} \sin 2\phi_{\rm PMT}}{\Sigma n_{\rm ch} \cos 2\phi_{\rm PMT}} \qquad (2)$$

where $n_{\rm ch}$ is the number of charged particles per PMT (determined from the pulse height in each PMT) and $\phi_{\rm PMT}$ is the azimuthal angle of each PMT. Then, it is calculated by the Fourier moment $v_2 = \langle \cos\ 2(\phi - \Phi_{\rm RP}) \rangle$ over all particles, for all events in a given sample [11]. Corrections [11–14] are applied to account for finite resolution in the reaction plane determination, and for possible azimuthal asymmetries in the reaction plane detector response. The bottom-left panel in Fig. 1 shows the average cosine of the difference between the two reaction planes defined by the beam counters at $\eta = 3 \sim 4$ and at $\eta = -4 \sim -3$ using the the elliptic (second) moment definition. In order to improve the reaction plane resolution, a combined reaction plane is defined by averaging the reaction plane angles obtained from each BBC, using the elliptic moment in each. The estimated resolution of the combined reaction plane [11], $\langle \cos\ 2(\Phi_{\rm measured} - \Phi_{\rm true}) \rangle$, has an average of 0.3 over centrality with a maximum of about 0.4. The estimated correction factor, which is the inverse of the resolution for the combined reaction plane, is shown in the top-left panel in Fig. 1.

The present technique is distinguished by defining the reaction plane angle using particles at high rapidity when measuring v_2 for particles at mid-rapidity. Other measurements of v_2 for mid-rapidity particles at RHIC have used reaction planes defined with mid-rapidity particles; or have employed a technique of measuring angular correlations between pairs of particles at mid-rapidity. While these different approaches generally seek to measure the same thing, they are not identical and a variety of physics effects can cause them to yield different results from the same collision sample [15,16,4]. Because of the large rapidity gap between the reaction plane and the mid-rapidity acceptance of about 3 units, it is expected that this analysis is less affected by non-flow contributions. However, we do not observe any substantial difference between the v_2 results shown here and published results for the v_2 of charged particles at RHIC in the $p_{\rm T}$ range where they are available.

The centrality of each collision is defined using the simultaneous measurement of the total number of particles measured in the BBC and the total energy measured in the zero degree calorimeter [17]. The middle panel in Fig. 1 shows the centrality dependence of v_2 for charged

particles measured at mid-rapidity ($|\eta| < 0.35$) with respect to the reaction plane defined above. The centrality is measured in percentile from the most central collision. The v_2 parameter decreases for both peripheral and central collisions with a maximum at about 50% of the geometric cross section. Beyond 70%, the correction factor due to the reaction plane resolution is large, as shown the left-most panel in the Fig. 1. This limits the centrality range used in this analysis.

The right-most panel in Fig. 1 shows the transverse momentum dependence of v_2 for charged particles with respect to the reaction plane for minimum-bias events. The data above a $p_{\rm T}$ of 2 GeV/c clearly show a deviation from the monotonically increasing behavior seen at smaller $p_{\rm T}$. The systematic errors are shown as line bands, which are estimated by several reaction plane methods using the two single beam counters or combined beam counters and by several different ways to correct non-uniform reaction plane distribution: "inverse weighting," "re-centering of sine and cosine summation," "Fourier expansion" and combinations of those above [11,18]. Those systematic errors are estimated to be about 10%, depending on centrality, and are independent of $p_{\rm T}$. Above 3 GeV/c, background tracks result in an additional systematic error of about 10%, depending on $p_{\rm T}$, which is included in the upper error band [19].

In Fig. 2, the transverse momentum dependence of v_2 for identified particles is shown. The top-left panel shows negatively charged particles, while the top-right panel shows positively charged particles as described in the figure caption. The statistical errors and the systematic errors are plotted independently. From the lambda particle spectra measured in the PHENIX central arm, it is determined that approximately 35% of the protons originate from lambda decays ("lambda feed-down") [20]. The effect of the lambda feed-down on the measured v_2 of the proton is studied by varying the lambda v_2 with Monte Carlo simulation. Protons resulting from lambda feed-down increase the measured v_2 value. Using the value of the lambda v_2 measured at $\sqrt{s_{\rm NN}} = 130$ GeV at RHIC [3], the effect on the proton v_2 would be less than 10%. Less than 5% of protons originate from decays of particles not involving the lambda. Based on further simulations of their decays to protons, we estimate that the total systematic error due to feed-down is at most 11% depending on $p_{\rm T}$, which is included in the lower sytematic error band in Fig. 2.

The combined positive and negative particles are shown in the bottom-left panel. The lines in that panel represent a hydrodynamical calculation [21] including a first-order phase transition with a freeze-out temperature of 120 MeV. The data show that at lower $p_{\rm T}$ (< 2 GeV/c), the lighter mass particles have a larger v_2 at a given $p_{\rm T}$, which is reproduced by the model calculations. We note, however, that the difference between the charged kaons and charged pions is larger than the model predicts.

A striking feature observed at higher $p_{\rm T}$ is that the v_2 of p and $\overline{p}$ are larger than for π and K at $p_{\rm T} > 2$ GeV/c. This is in sharp contrast to the hydrodynamical picture, which would predict the same mass-ordering for v_2 at all $p_{\rm T}$. In our data the mesons begin to show a departure from the hydrodynamical prediction at $p_{\rm T}$ of about 1.5 GeV/c, while the (anti)baryons agree with the prediction up until 3 GeV/c but may be deviating at higher $p_{\rm T}$. Such behavior is predicted by the quark coalescence mechanism [22], as shown in the bottom-right panel where both v_2 and $p_{\rm T}$ have been scaled by the number of quarks. This could be an indication that the v_2 of measured hadrons is already established in a quark-matter phase, although it does not explain why the quark v_2 would saturate with $p_{\rm T}$. There exist other scenarios that could be applicable at RHIC, but we have selected two simple models (hydrodynamical and quark coalesence) only to emphasize the experimental evidence of the crossing of v_2 for mesons and baryons.

As an additional illustration of the different behavior for mesons and baryons, the transverse momentum dependences of the v_2 parameter are shown in Fig. 3 for different particles and different centralities. Since the particle identification separation of K and p goes up to 4 GeV/c, the combined π and K can be compared with protons up to 4 GeV/c. The charged particle acceptance is larger than the TOF acceptance where the particle identification can be performed. Therefore, the statistical fluctuations for the charged particle v_2 are smaller than for the p, $\overline{p}$ and $\pi+K$. The trend exhibited in Fig. 2 for minimum bias spectra, in which the v_2 parameter for (anti)baryons exceed those for mesons at $p_{\rm T} > 2$ GeV/c, is shown here to occur for all centralities.

In summary, the value of the v_2 parameter for identified and inclusive charged particle production at mid-rapidity has been measured with respect to the reaction plane defined in the forward and backward rapidity regions in $\sqrt{s_{\rm NN}} = 200$ GeV Au+Au collisions, using the PHENIX experiment at RHIC. The value of v_2 for charged particles decreases for both peripheral and central collisions with a maximum at about the $50^{\rm th}$ percentile of the geometric cross section. We have observed that for charged particles v_2 increases with $p_{\rm T}$ up to about 2 GeV/c, then starts to saturate or decrease slightly. However, the detailed behavior is different for different particle species. The lighter particles have larger v_2 than the heavier particles for $p_{\rm T}$ below 2 GeV/c. This trend is partly reversed above 2 GeV/c where the proton and anti-proton have larger v_2 than mesons, a pattern which persists over all centralities. A hydrodynamical calculation can reproduce the mass-ordering and magnitude of v_2 for the different particles in the region up to 2 GeV/c, but fails to reproduce either in the $p_{\rm T}$ region above 2 GeV/c. As an alternative, we investigated the quark-coalescence scenario, in which the anisotropy

of the final-state hadrons is largely inherited from the anisotropy of quarks in a preceding quark-matter phase. The quark-coalescence model makes a definite prediction for a simple scaling behavior between the v_2 for mesons and for (anti)baryons, and this scaling behavior is largely, though not perfectly, borne out in our data. Further measurements extending to higher p_T involving more identified species will be required to discriminate among alternative scenarios for the origin of elliptic flow at RHIC.

We thank the staff of the Collider-Accelerator and Physics Departments at BNL for their vital contributions. We acknowledge support from the Department of Energy and NSF (U.S.A.), MEXT and JSPS (Japan), CNPq and FAPESP (Brazil), NSFC (China), CNRS-IN2P3 and CEA (France), BMBF, DAAD, and AvH (Germany), OTKA (Hungary), DAE and DST (India), ISF (Israel), KRF and CHEP (Korea), RAS, RMAE, and RMS (Russia), VR and KAW (Sweden), U.S. CRDF for the FSU, US-Hungarian NSF-OTKA-MTA, and US-Israel BSF.

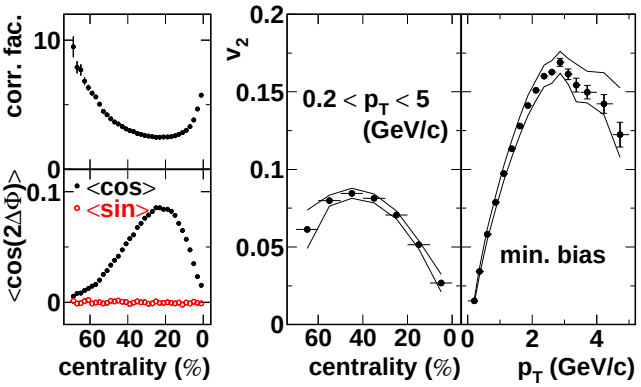

FIG. 1. (color online) Correlation of reaction planes between two beam counters for the second moment is shown as a function of centrality (bottom-left) and the correction factor for the combined reaction plane resolution of two beam counters is shown as a function of centrality (top-left). The value of v_2 for charged particles is shown as a function of centrality (middle) and as a function of p_T (right).

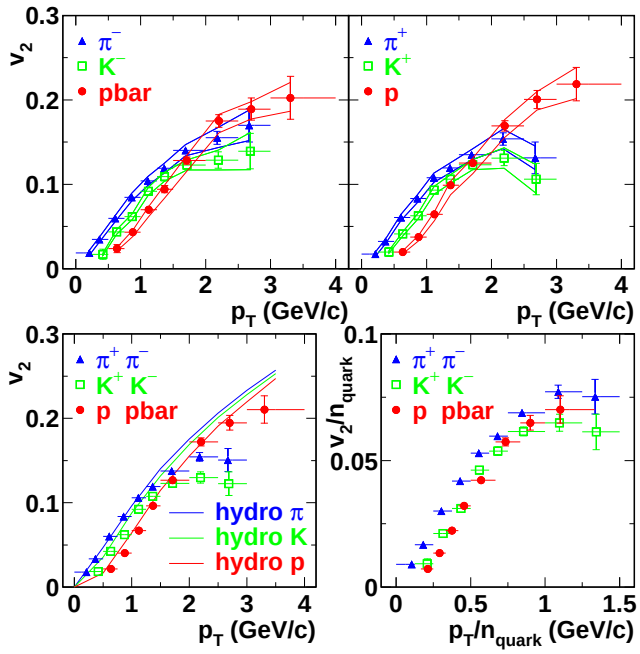

FIG. 2. (color online) Transverse momentum dependence of v_2 for identified particles, π^-, K^-, $\overline{p}$ (top-left) and π^+, K^+, p (top-right). The circles show p and $\overline{p}$, the squares show K^+ and K^-, and the triangles show π^+ and π^- for minimum bias events. Statistical errors are represented by error bars and overall systematic error due to all sources by the solid lines in the top two panels. The combined positive particles and negative particles are shown in the bottom-left panel, and the lines there represent the result of a hydrodynamical calculation [21] including a first-order phase transition with a freeze out temperature of 120 MeV for π, K and p from upper to lower curves, respectively. The bottom-right panel shows the quark v_2 as a function of the quark p_T by scaling both axes with the number of quarks for each particle, as motivated by a quark coalescence model [22].

* Deceased
† Spokesperson: zajc@nevis.columbia.edu

[1] K.H. Ackermann et al., Phys. Rev. Lett. **86**, 402 (2001).
[2] C. Adler et al., Phys. Rev. Lett. **87**, 182301 (2001).
[3] C. Adler et al., Phys. Rev. Lett. **89**, 132301 (2002).
[4] C. Adler et al., Phys. Rev. **C66**, 034904 (2002).
[5] C. Adler et al., Phys. Rev. Lett. **90**, 032301 (2003).
[6] K. Adcox et al., Phys. Rev. Lett. **89**, 212301 (2002).
[7] K. Adcox et al., Phys. Rev. Lett. **88**, 242301 (2002).
[8] K. Adcox et al., Nucl. Instrum. Methods in Phys. Research **A499**, 469 (2003).
[9] J. T. Mitchell et al., Nucl. Instrum. Methods in Phys. Research **A482**, 491 (2002).
[10] H. Hamagaki et al., Nucl. Phys. **A698**, 412 (2002).
[11] A. Poskanzer and S. Voloshin, Phys. Rev. **C58**, 1671 (1998).
[12] J. Barrette et al., Phys. Rev. Lett. **73**, 2532 (1994).
[13] J. Barrette et al., Phys. Rev. **C55**, 1420 (1997).
[14] J. Barrette et al., Phys. Rev. **C56**, 3254 (1997).
[15] N. Borghini, P.M. Dinh and J.Y. Ollitrault, Phys. Rev. **C63**, 054906 (2001).
[16] N. Borghini, P.M. Dinh and J.Y. Ollitrault, Phys. Rev. **C64**, 054901 (2001).
[17] K. Adcox et al., Phys. Rev. Lett. **86**, 3500 (2001).
[18] S. Esumi et al., Nucl. Phys. **A715**, 599 (2003).
[19] K. Adcox et al., Phys. Rev. Lett. **88**, 022301 (2002).
[20] K. Adcox et al., Phys. Rev. Lett. **89**, 092302 (2002).
[21] P. Huovinen, P.F. Kolb, U.W. Heinz, P.V. Ruuskanen and S.A. Voloshin, Phys. Lett. **B503**, 58 (2001).
[22] D. Molnar and S. Voloshin, nucl-th/0302014.

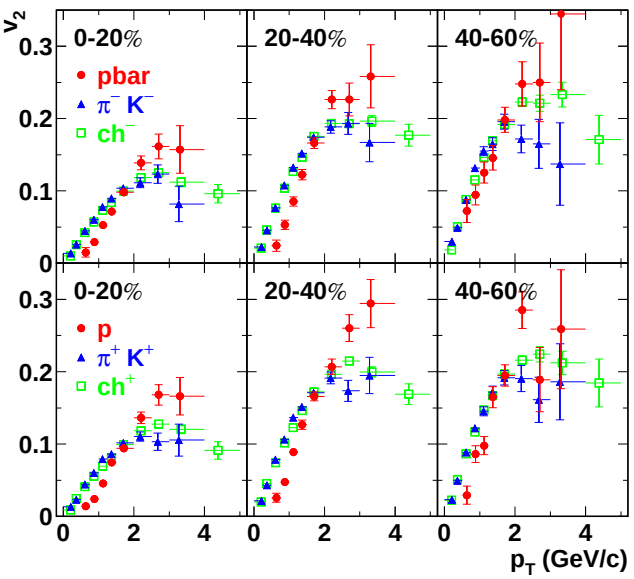

FIG. 3. (color online) Transverse momentum dependence of v_2 for combined π^- and K^- (top) or π^+ and K^+ (bottom) compared with $\overline{p}$ (top) and p (bottom). In addition, results for inclusive negative (top) and positive (bottom) charged particle distributions are plotted as open squares. From the left to right, the different centrality selections are shown for 0-20% (left), 20-40% (middle) and 40-60% (right).